^{89}Zr-anti-γH2AX-TAT but not ^{18}F-FDG allows early monitoring of response to chemotherapy in a mouse model of pancreatic ductal adenocarcinoma

James C. Knight[1], Michael Mosley[1], Luisa Contreras Bravo[1], Veerle Kersemans[1], Danny Allen[1], Somnath Mukherjee[1], Eric O'Neill[1], and Bart Cornelissen[1†]

[1] CR-UK/MRC Oxford Institute for Radiation Oncology, Department of Oncology, University of Oxford, Oxford, United Kingdom

Word count: 5,318
Running title: Imaging DNA damage response in PDAC
Key words: γH2AX, Pancreatic Ductal Adenocarcinoma, PET, Molecular Imaging
Financial Support: This research was supported by Pancreatic Cancer UK, CRUK through the Oxford Institute for Radiation Oncology and the CRUK Oxford Centre, and the CRUK/EPSRC Imaging Centre in Oxford.

The authors disclose no potential conflicts of interest

[†] **To whom correspondence should be addressed:**
Dr. Bart Cornelissen
CRUK/MRC Oxford Institute for Radiation Oncology
Department of Oncology
University of Oxford
Old Road Campus Research Building
Off Roosevelt Drive
Oxford OX3 7LJ
Tel: +44 (0)1865 857126
Fax: +44 (0)1865 857127
Email: bart.cornelissen@oncology.ox.ac.uk

Abstract

Purpose: Late-stage, unresectable pancreatic ductal adenocarcinoma (PDAC) is largely resistant to chemotherapy and consequently has a very poor 5-year survival rate of < 5%. The ability to assess the efficacy of a treatment soon after its initiation would enable rapid switching to potentially more effective therapies if the current treatment is found to be futile. We have evaluated the ability of the PET imaging agent, ^{89}Zr-anti-γH2AX-TAT, to monitor DNA damage in response to fluouracil (5-FU), gemcitabine, or capecitabine treatment in a mouse model of pancreatic cancer. We have also compared the utility of this approach against the standard clinical PET radiotracer, ^{18}F-FDG.

Experimental Design: C57BL/6 mice bearing subcutaneous pancreatic cancer (KPC; B8484) allografts were treated with 5-FU, gemcitabine, or capecitabine. Therapeutic response was monitored by positron emission tomography and *ex vivo* biodistribution experiments using either ^{89}Zr-anti-γH2AX-TAT or ^{18}F-FDG as imaging agents. To further examine the effect of therapeutic response upon uptake of these imaging agents, immunohistochemical analysis of harvested tumour allograft tissue was also performed.

Results: Accumulation of ^{89}Zr-anti-γH2AX-TAT in the tumours of mice that received chemotherapy was higher compared with vehicle-treated mice and was shown to be specifically mediated by γH2AX. In contrast, ^{18}F-FDG did not provide useful indications of therapeutic response.

Conclusions: ^{89}Zr-anti-γH2AX-TAT has shown a superior ability to monitor early therapeutic responses to chemotherapy by PET imaging compared with ^{18}F-FDG in an allograft model of PDAC in mice.

Statement of Translational Relevance

Current chemotherapy regimens for pancreatic ductal adenocarcinoma do not appreciably prolong patient survival due to intrinsic or rapidly acquired resistance. To improve survival outcomes it is therefore critical to determine whether a patient is responding to treatment as early as possible so that a futile treatment can be quickly replaced with one which is more effective. Monitoring response to therapy by PET is attractive as this imaging technique can detect the early molecular indications of treatment efficacy. The standard clinical PET imaging agent is ^{18}F-FDG which despite its widespread use has several limitations, including a tendency to accumulate non-specifically in areas of inflammation and an inability to differentiate focal mass-forming pancreatitis from pancreatic cancer. As most chemotherapy agents are designed to cause DNA damage, we propose that monitoring the DNA damage response with the PET imaging agent ^{89}Zr-anti-γH2AX-TAT would provide a more direct measure of treatment efficacy.

INTRODUCTION

At present, less than 5% of patients diagnosed with pancreatic cancer will survive longer than 5 years.(1) This poor prognosis is due in part to a lack of screening measures which result in most patients being diagnosed when the disease is in an advanced, metastatic state. Consequently, the opportunity for potentially curative surgical resection has usually been missed and the patient is typically offered chemo- and/or radiotherapy, or palliative treatments.(2) Standard chemotherapy regimens for advanced pancreatic cancer include gemcitabine, fluorouracil (5-FU), capecitabine, Nab-paclitaxel (Abraxane) and FOLFIRNOX. Response to single agent chemotherapy is typically less than 10%, and response to multi-agent chemotherapy (gemcitabine/nab-Paclitaxel and FOLFIRNOX) in the region of 25-30%.(3-5) The limited efficacy of these treatments with regard to prolonging patient survival is largely due to intrinsic or acquired resistance to these agents.(6,7) The ability, therefore, to monitor the efficacy of a particular chemotherapy early on during treatment would be advantageous as a futile treatment could be rapidly switched to an alternative therapy.

The conventional methods for assessing response to therapy are based on ~~the Response Evaluation Criteria in Solid Tumours (RECIST) guidelines~~anatomical assessment of tumor size ~~which rely upon physical measurements of tumour dimensions determined~~ by X-ray, computed tomography (CT) or magnetic resonance imaging (MRI).(8,9) More recently, molecular imaging techniques including positron emission tomography (PET) and single-photon emission computed tomography (SPECT) have also been recognised as valuable tools for evaluating treatment response.(10-13) These imaging techniques allow visualisation and quantitation of cellular and biochemical responses to treatment which can indicate the efficacy of therapy soon after its initiation and before changes in tumour dimensions can be measured.

The clinical PET imaging agent fluorodeoxyglucose (^{18}F-FDG) accumulates in tumour tissue due to an increased reliance on glycolysis for energy production even under normoxic conditions compared with normal cells (*i.e.* the Warburg effect).(14-16) Like glucose, ^{18}F-FDG is internalised *via* glucose transporters (particularly GLUT-1 and GLUT-3) and is then phosphorylated by

hexokinase. However, unlike glucose-6-phosphate, the newly formed ^{18}F-FDG-6-phosphate is resistant to subsequent enzymatic metabolism and is retained within the cell, resulting in specific accumulation of the imaging agent within tumours. In addition to its roles in cancer detection and staging, ^{18}F-FDG has also been used successfully for monitoring response to various forms of therapy in many cancer types(17-25), including pancreatic ductal adenocarcinoma (PDAC).(26-28)

While the use of ^{18}F-FDG for monitoring therapy is showing significant promise, this imaging agent has several well-recognised limitations, particularly relating to pancreatic cancer.(29-33) These limitations include the occurrence of non-specific uptake of ^{18}F-FDG in inflammatory lesions and regions of infection, and an inability to reliably distinguish focal mass-forming pancreatitis from pancreatic cancer.

A more direct strategy for monitoring treatment efficacy involves gauging molecular effects such as the DNA damage response (DDR) which is activated in response to most chemotherapy agents.(34-36) At present, in clinical settings this can be accomplished by performing immunohistochemical analysis of biopsied tissues.(37) However, recovery of tissue biopsies is an invasive procedure which can pose risks of haemorrhaging and infection. Furthermore, biopsies prevent longitudinal assessment *via* repeated monitoring of the same region and offer only limited insights into tumour heterogeneity. Therefore, the ability to probe for biomarkers of DDR non-invasively *via* PET or SPECT imaging is an attractive prospect.

A well-established biomarker of DDR is the phosphorylated histone γH2AX which forms foci around double-strand breaks (DSBs) of DNA.(37,38) γH2AX arises in response to DNA DSBs when members of the phosphoinositide 3-kinase-related protein kinase family (including ATM, ATR, and DNA-PKcs) phosphorylate the X isoform of H2A at the serine-139 position.(39,40) Thereafter, γH2AX mediates the repair of DNA DSBs by recruiting several other DNA repair proteins to the damaged site.(41,42)

Research efforts are currently underway to develop a non-invasive means of quantifying γH2AX expression levels *in vivo* using both PET and SPECT imaging techniques.(43-45) Previously,

we showed that the uptake of ~~We recently developed~~ an antibody-based SPECT imaging agent, ^{111}~~^{89}~~In~~Zr~~-anti-γH2AX-TAT, in MDA-MB-468 xenograft tumors in mice was linearly dependent on the number of γH2AX foci per cell, and linearly dependent on radiation deposited dose after gamma-irradiation of the tumour.(43) More recently, we have developed an analogous imaging agent containing the PET radioisotope ^{89}Zr which was successful in detecting elevated levels of γH2AX following radiation-induced DNA damage in breast cancer xenografts in mice.(45) In the present study, we sought to investigate whether ^{89}Zr-anti-γH2AX-TAT can be used to monitor the activation of DDR in response to three standard chemotherapy agents in a mouse allograft model of PDAC and have performed a comparison with ^{18}F-FDG.

METHODS AND MATERIALS

General Methods

All reagents were purchased from Sigma-Aldrich unless otherwise stated and were used without further purification. The chelating agent *p*-SCN-Bn-DFO was purchased from Macrocyclics Inc. (Dallas, TX). Water was deionised using a Barnstead NANOpure purification system (Thermo Scientific) and had a resistance of >18.2 MΩ cm^{-1} at 25 °C. Protein concentration measurements were made on a ND-1000 spectrophotometer (NanoDrop Technologies, Inc.). Instant thin-layer chromatography (iTLC) was performed on glass microfiber chromatography paper (Agilent Technologies) and strips were analysed with either a Bioscan AR-2000 radio-TLC scanner (Eckert & Ziegler) or a Cyclone Plus Phosphor Imager (PerkinElmer). pH was determined using pH indicator paper (Merck Millipore). Radioactivity measurements were made using a CRC®-25R dose calibrator (Capintec, Inc.).

Cell culture

KPC cells (B8484) were derived from Kras$^{LSL-G12D/+}$; Trp53$^{LSL-R172H/+}$; Pdx1-Cre (KPC) tumours. Cells were maintained in Dulbecco's Modified Eagle Medium (DMEM), supplemented with 10% foetal

bovine serum (FBS), 2 mM L-glutamine, 100 units/mL penicillin, and 0.1 mg mL^{-1} streptomycin. Cells were grown in a 37°C environment containing 5% CO_2 and were harvested and passaged as required using Trypsin-EDTA solution. The cumulative length of culture was less than 6 months following retrieval from liquid nitrogen storage.

Preparation of ^{89}Zr-anti-γH2AX-TAT

Anti-γH2AX (DR1017, Merck Millipore) was modified with the cell-penetrating peptide TAT (GRKKRRQRRRPPQGYG) by a previously described method.(43) Modification of anti-γH2AX-TAT with *p*-SCN-Bn-DFO and subsequent radiolabelling with zirconium-89 were conducted using previously reported methods.(46) In brief, to a solution of γH2AX-TAT (200 µg) or rabbit IgG (200 µg, I5006, Sigma Aldrich) in 0.1 M $NaHCO_3$ (pH 8.9, 125 µL, Chelex treated) was added 10 molar equivalents of *p*-SCN-Bn-DFO (6.64 mM) in anhydrous dimethyl sulfoxide. The reaction mixture was incubated at 37°C for 60 minutes with gentle shaking (450 rpm) and the excess *p*-SCN-Bn-DFO was removed by Sephadex-G50 size exclusion chromatography.

Zirconium-89 in 1 M oxalic acid (sourced from VU Amsterdam) was adjusted to pH 7 by the addition of 1 M sodium carbonate. The resulting solution was added to a 2 mg mL^{-1} solution of the DFO-modified antibody to achieve a ratio of 0.1 MBq to 1 µg. The reaction mixture was incubated at room temperature for 1 h and the radiolabeling efficiency was determined by iTLC using an eluent of 50 mM ethylenediaminetetraacetic acid (EDTA) buffer (pH 6). The crude reaction mixture was purified by Sephadex-G50 size exclusion chromatography, eluting with 100 µL fractions of phosphate buffered saline (PBS; pH 7.4).

^{89}Zr-labelled TAT-modified rabbit IgG (RIgG-TAT) was used as a negative control, and synthesised from rabbit IgG as described above for ^{89}Zr-anti-γH2AX-TAT.

In vivo studies

All animal procedures were performed in accordance with the UK Animals (Scientific Procedures) Act 1986 and with local ethical committee approval. Allograft tumours were established in the right hind flank of female C57BL/6 mice by subcutaneous injection of 1×10^6 KPC cells in PBS (100 µL). Tumour volumes (V) were calculated after calliper measurement using the following equation: $V = (a^2 \times b)/2$, where a is the width of the tumour and b the length (small and large diameters, respectively). The individual relative tumour volume (RTV) was defined as Vt/V_0, where Vt is the volume at a given time and V_0 at the start of treatment.

PET/CT imaging experiments

PET/CT images were acquired using an Inveon PET/CT scanner (Siemens Preclinical Solutions). For full experimental details and acquisition parameters, see Supporting Information. Therapy and imaging regimens are summarised in Figs. 1, 2, 3 and 4, and are described in full in the Supporting Information.

Ex vivo biodistribution experiments

Mice were euthanized by cervical dislocation and selected organs, tissues and blood were removed. The samples were immediately rinsed with water, dried, and transferred into a pre-weighed counting tube. After weighing the filled counting tubes, the amount of radioactivity in each was measured using a 2480 WIZARD^2 or 1470 WIZARD gamma counter (PerkinElmer). Counts per minute were converted into radioactivity units (MBq) using calibration curves generated from known standards. These values were decay-corrected to the time of injection, and the percentage of the injected dose per gram (%ID/g) of each sample was calculated.

Immunohistochemical staining for GLUT-1 and γH2AX

Sections of tumour allograft tissue were obtained at 7 µm thickness using a cryostat (OTF5000, Bright Instruments). Tissue sections were fixed in 4% paraformaldehyde for 10 minutes at room temperature, washed twice in PBS, then permeabilized in 1% triton/PBS for 10 minutes at room temperature. After

rinsing in PBS, tissue sections were incubated with blocking buffer (2% bovine serum albumin/0.1% Triton in PBS) for 1 h at room temperature and then incubated with the relevant primary antibody (anti-GLUT-1 rabbit pAb [1:250 dilution, ab652, Abcam] or anti-γH2AX rabbit pAb [1:800 dilution, DR1017 (Gemcitabine and Capecitabine experiments) or 07-164 (5-FU experiments), Merck Millipore] overnight at 4°C. After washing with PBS, tissue sections were then incubated with fluorescently-labelled secondary Goat-Rabbit IgG-Dylite 488 (1:250 dilution in blocking buffer) for 1 h at room temperature. After washing with PBS, slides were mounted with VECTASHIELD mounting medium with DAPI (Vector labs, Peterborough, UK). Confocal microscopy images were acquired using a Zeiss 530 microscope (Zeiss, Welwyn Garden City, UK). Standardized relative quantification of GLUT-1 and γH2AX immunofluorescence was performed by normalising the Dylite 488 signal intensity to the DAPI signal.

Statistical Analyses

All statistical analyses and nonlinear regression were performed using GraphPad Prism (GraphPad Software, San Diego, CA, USA). Data were tested for normality and analysed either by the unpaired, two-tailed Student's t-test where appropriate, or 1-way analysis of variance (ANOVA) for multiple comparisons, with ~~Tukey~~Dunnet's post-tests to calculate significance of differences between groups. All data were obtained at least in triplicate and results reported as mean ± standard deviation, unless stated otherwise.

RESULTS

Zirconium-89 radiolabelling of DFO-anti-γH2AX-TAT

^{89}Zr-anti-γH2AX-TAT and ^{89}Zr-RIgG-TAT were routinely synthesized in high radiochemical yields (87.7±13.5% and 85.2±14.5%, respectively) and obtained in excellent purity (>99%) following G50 size-exclusion chromatography. See Fig. S1 for representative iTLC chromatograms.

Tumour uptake and radiotracer distribution

5-FU therapy

PET/CT images acquired three days after a single dose of 5-FU revealed higher uptake of ^{89}Zr-anti-γH2AX-TAT in tumours of treated mice compared with experimental controls (Fig. 1A). Within this timeframe, the growth rate of KPC allografts in mice treated with a single dose of 5-FU was not significantly impeded compared with vehicle-treated mice (Fig. 1B). Values obtained from *ex vivo* biodistribution experiments at 24 h p.i. revealed that uptake of ^{89}Zr-anti-γH2AX-TAT in the tumours of treated mice reached a value of 8.5±1.1 %ID/g (Table S1) which was higher than the vehicle-treated mice and mice administered an imaging agent lacking γH2AX specificity, ^{89}Zr-RIgG-TAT (P<0.01; Table S1). These observations correlate well with immunohistochemical analysis of the harvested tumour allograft tissues (Fig. 1D and Fig 1E) as significantly higher expression levels of γH2AX were measured in the tumours of 5-FU treated mice compared with tumours of vehicle-treated mice (67±19 and 49±21 a.u., respectively; P<0.05).

Similar PET/CT imaging experiments with ^{18}F-FDG did not reveal any differences in tumour uptake after initiation of 5-FU treatment either at an early stage (Day 3) before any effect upon RTV was observed, or on Day 9 when the mean RTV of treated mice was significantly smaller than vehicle-treated mice (Fig. 2A-C). *Ex vivo* biodistribution analysis performed immediately after the final imaging session on Day 9 (Table S2) and immunohistochemical staining of harvested tumours confirmed these results and showed no significant difference in GLUT-1 expression levels (Fig. 2D and 2E).

Gemcitabine therapy

PET/CT images acquired 3 days after a single administration of gemcitabine revealed higher uptake of ^{89}Zr-anti-γH2AX-TAT in the tumours of gemcitabine-treated mice compared with the non-specific controls (Fig. 3A). Within this timeframe there was no significant difference in mean RTV compared with a vehicle-treated control cohort of mice (Fig 3B). Analysis of the *ex vivo* biodistribution data (Table S3) indicated that uptake of ^{89}Zr-anti-γH2AX-TAT in the tumours of gemcitabine-treated mice reached a value of 6.8±0.6 %ID/g and was significantly higher than experimental controls (Fig. 3C;

P<0.01, Table S3). Confocal microscopy images obtained from tumour tissue sections revealed higher γH2AX expression levels in the tumours of gemcitabine-treated mice compared with tumours harvested from vehicle-treated mice (67±30 and 40±13 a.u., respectively; *P*<0.05) (Figs. 3D and 3E).

In a similar fashion to the 5-FU therapy experiments, PET images acquired with ^{18}F-FDG did not reveal any significant difference in tumour uptake between gemcitabine- and vehicle-treated mice at Day 3 (before any effect on RTV was observed) or Day 8 when a significant difference in RTV between these groups could be measured (Fig. 4A-C). Interestingly, analysis of the *ex vivo* biodistribution data acquired immediately after the final imaging session on Day 8 (Table S4) revealed significantly higher uptake of ^{18}F-FDG in the tumours of gemcitabine-treated mice compared with vehicle-treated mice (7.6±1.5 and 3.3±2.0 %ID/g, respectively; *P*<0.05). Conversely, analysis of confocal microscopy images (Figs. 5D and 5E) indicated that GLUT-1 expression levels were reduced in the tumours of gemcitabine-treated mice (96±40 a.u.) compared with vehicle-treated mice (65±44 a.u.; *P*<0.05)

Capecitabine therapy

The results of the capecitabine experiments with ^{89}Zr-anti-γH2AX-TAT and ^{18}F-FDG which showed similar trends but did not reach statistical significance are provided in full in the supporting information.

DISCUSSION

^{89}Zr-anti-γH2AX-TAT was effective in detecting upregulation of γH2AX in each of the applied chemotherapy regimens. Notably, in all cases, the detection of treatment-induced γH2AX upregulation preceded a change in relative tumour volume compared with vehicle-treated control mice. In contrast, VOI analysis of PET images indicated that uptake of ^{18}F-FDG within tumours did not change as a result of any of the administered chemotherapies, either soon after the initiation of therapy or following completion of therapy. This observation is notable, particularly in the case of 5-

FU and gemcitabine-treated mice which experienced significant impediment of tumour growth compared with vehicle-treated mice. It would be reasonable to expect the rate of glucose metabolism to be reduced in the tumours of mice treated with chemotherapy, and indeed this was partially reflected by a reduction in the expression levels of GLUT-1 in tumours harvested from gemcitabine-treated mice. However, in mice treated with 5-FU or capecitabine, no signification reduction in GLUT-1 expression levels was observed. This supports our contention that compared with measuring changes in glucose metabolism, it is of more value to monitor the effects of DNA damaging treatments in a more direct manner by tracking the upregulation of key DNA repair proteins, such as γH2AX.

^{89}Zr-anti-γH2AX-TAT is one of a small number of PET imaging agents that have demonstrated the ability to track DDR proteins during cancer therapy in preclinical studies. Other recent examples include radiolabelled small molecule inhibitors of PARP-1, such as ^{18}F-BO which showed substantially decreased uptake in A2780 human ovarian cancer xenograft tumours in mice following treatment with Olaparib.(47) While PARP-1 is principally involved in the repair of single-strand breaks in DNA, γH2AX is mostly upregulated in response to DNA DSBs which require longer repair times. In principle, targeting more slowly dissipating epitopes such γH2AX may provide an extended time window during which useful PET imaging measurements of therapy response can be obtained.

Although significant differences can be observed following chemotherapy, for each of the chemotherapy regimens it can be observed that a ~~significant~~ proportion of the overall uptake of ^{89}Zr-anti-γH2AX-TAT is non-specific and is consistent with uptake levels expected from the enhanced permeability and retention (EPR) effect(48,49). This phenomenon is caused by the leaky vasculature within tumours which causes high molecular weight species such as ^{89}Zr-anti-γH2AX-TAT to passively extravasate to tumour tissue. In order to overcome this limitation, future investigations will be focused on amplifying the proportion of γH2AX-mediated signal by, for example, utilisation of lower molecular weight targeting vectors (to diminish the EPR effect(50)), ~~pretargeting strategies (to improve T/B contrast ratios(51))~~, and molecularly-targeted CPPs (to improve tumour targeting(52)).

CONCLUSIONS

It has been demonstrated that the PET imaging agent ^{89}Zr-anti-γH2AX-TAT is capable of monitoring the induction of γH2AX that occurs as a result of chemotherapy in an allograft model of PDAC in mice. Notably, ^{89}Zr-anti-γH2AX-TAT has shown a superior ability to provide early indications of therapy response compared with the standard clinical PET radiotracer, ^{18}F-FDG. Despite being commonly used to evaluate response to therapy in patients with pancreatic cancer, we found that ^{18}F-FDG did not provide any indication of therapeutic response either soon after initiation of treatment or following its completion. Furthermore, in cases where a reduction of GLUT-1 expression was observed in tumours following treatment, this was not accompanied by a reduction of ^{18}F-FDG uptake, indicating that overall uptake of ^{18}F-FDG was dominated by a non-specific contribution. In contrast, ^{89}Zr-anti-γH2AX-TAT offers a highly sensitive and more direct means of monitoring response to DNA damaging therapies.

ACKNOWLEDGEMENTS

This research was supported by the CRUK through the Oxford Institute for Radiation Oncology and the CRUK Oxford Centre, and the CRUK/EPSRC Imaging Centre in Oxford. S. Mukherjee is part funded by NIHR Oxford Biomedical Research Centre. We also thank David Y. Lewis, Ferdia A. Gallagher, Deborah Sneddon and Julia Baguña Torres for helpful discussions in the preparation of this manuscript. Lastly, we wish to thank Fergus Gleeson and Paul Murphy at the Oxford University Hospitals NHS Foundation Trust for providing ^{18}F-FDG.

Authors' Contributions

Conception and design: B. Cornelissen, S. Mukherjee, E. O'Neill

Radiochemistry: J. Knight

In vivo imaging experiments: J. Knight, V. Kersemans

Ex vivo biodistribution experiments: J. Knight, L. Contreras Bravo

Immunohistochemistry: L. Contreras Bravo, M. Mosley, J. Knight,

Analysis, image processing, and interpretation of data: J. Knight, D. Allen, B. Cornelissen

Writing, review, and/or revision of the manuscript: J. Knight, B. Cornelissen

Study supervision: B. Cornelissen

FIGURE LEGENDS

Fig. 1 Monitoring 5-FU therapy with ^{89}Zr-anti-γH2AX-TAT: (A) PET/CT images showing coronal (upper) and transaxial (lower) sections intersecting the centre of the allograft tumour (white dotted circle), (B) Tumour growth curve, (C) Tumour uptake values obtained from *ex vivo* biodistribution experiments, * = P<0.05 (D) Representative confocal microscopy images, 63x (blue: DAPI, green: γH2AX), (E) Quantification of γH2AX signal on confocal microscopy images normalised to DAPI signal, * = P<0.05. Error bars represent standard error of the mean.

Fig. 2 Monitoring 5-FU therapy with ^{18}F-FDG: (A) PET/CT images showing coronal (upper) and transaxial (lower) sections intersecting the centre of the allograft tumour (white dotted circle), (B) Tumour growth curve, (C) Tumour uptake values obtained from VOI analysis, (D) Representative confocal microscopy images, 20x (blue: DAPI, green: γH2AX), (E) Quantification of GLUT-1 signal on confocal microscopy images normalised to DAPI signal. Error bars represent standard error of the mean.

Fig. 3 Monitoring gemcitabine therapy with ^{89}Zr-anti-γH2AX-TAT: (A) PET/CT images showing coronal (upper) and transaxial (lower) sections intersecting the centre of the allograft tumour (white dotted circle), (B) Tumour growth curve, (C) Tumour uptake values obtained from *ex vivo* biodistribution experiments, * = P<0.05 (D) Representative confocal microscopy images, 63x (blue: DAPI, green: γH2AX), (E) Quantification of γH2AX signal on confocal microscopy images normalised to DAPI signal, * = P<0.05. Error bars represent standard error of the mean.

Fig. 4 Monitoring gemcitabine therapy with ^{18}F-FDG: (A) PET/CT images showing coronal (upper) and transaxial (lower) sections intersecting the centre of the allograft tumour (white dotted circle), (B) Tumour growth curve, ** = P<0.01 (C) Tumour uptake values obtained from VOI analysis, (D) Representative confocal microscopy images, 20x (blue: DAPI, green: γH2AX), (E) Quantification of GLUT-1 signal on confocal microscopy images normalised to DAPI signal, * = P<0.05. Error bars represent standard error of the mean.

REFERENCES

1. Hidalgo M. Pancreatic Cancer. N Engl J Med **2010**;362(17):1605-17 doi 10.1056/NEJMra0901557.
2. Huguet F, Girard N, Guerche CS-E, Hennequin C, Mornex F, Azria D. Chemoradiotherapy in the Management of Locally Advanced Pancreatic Carcinoma: A Qualitative Systematic Review. J Clin Oncol **2009**;27(13):2269-77 doi 10.1200/JCO.2008.19.7921.
3. Burris HA, Moore MJ, Andersen J, Green MR, Rothenberg ML, Modiano MR, *et al.* Improvements in survival and clinical benefit with gemcitabine as first-line therapy for patients with advanced pancreas cancer: a randomized trial. J Clin Oncol **1997**;15(6):2403-13 doi 10.1200/JCO.1997.15.6.2403.
4. Conroy T, Desseigne F, Ychou M, Bouché O, Guimbaud R, Bécouarn Y, *et al.* FOLFIRINOX versus Gemcitabine for Metastatic Pancreatic Cancer. New England Journal of Medicine **2011**;364(19):1817-25 doi 10.1056/NEJMoa1011923.
5. Von Hoff DD, Ervin T, Arena FP, Chiorean EG, Infante J, Moore M, *et al.* Increased Survival in Pancreatic Cancer with nab-Paclitaxel plus Gemcitabine. N Engl J Med **2013**;369(18):1691-703 doi 10.1056/NEJMoa1304369.
6. Stathis A, Moore MJ. Advanced pancreatic carcinoma: current treatment and future challenges. Nat Rev Clin Oncol **2010**;7(3):163-72.
7. Wang Z, Li Y, Ahmad A, Banerjee S, Azmi AS, Kong D, *et al.* Pancreatic cancer: understanding and overcoming chemoresistance. Nat Rev Gastroenterol Hepatol **2011**;8(1):27-33.
8. Eisenhauer EA, Therasse P, Bogaerts J, Schwartz LH, Sargent D, Ford R, *et al.* New response evaluation criteria in solid tumours: Revised RECIST guideline (version 1.1). Eur J Cancer **2009**;45(2):228-47 doi http://dx.doi.org/10.1016/j.ejca.2008.10.026.
9. Wahl RL, Jacene H, Kasamon Y, Lodge MA. From RECIST to PERCIST: Evolving Considerations for PET Response Criteria in Solid Tumors. J Nucl Med **2009**;50(Suppl 1):122S-50S doi 10.2967/jnumed.108.057307.

10. Shankar LK, Hoffman JM, Bacharach S, Graham MM, Karp J, Lammertsma AA, *et al.* Consensus Recommendations for the Use of 18F-FDG PET as an Indicator of Therapeutic Response in Patients in National Cancer Institute Trials. J Nucl Med **2006**;47(6):1059-66.

11. Zhu A, Lee D, Shim H. Metabolic Positron Emission Tomography Imaging in Cancer Detection and Therapy Response. Semin Oncol **2011**;38(1):55-69 doi http://dx.doi.org/10.1053/j.seminoncol.2010.11.012.

12. Price P, Jones T. Can positron emission tomography (PET) be used to detect subclinical response to cancer therapy? Eur J Cancer **1995**;31(12):1924-7 doi http://dx.doi.org/10.1016/0959-8049(95)00421-1.

13. Gambhir SS. Molecular imaging of cancer with positron emission tomography. Nat Rev Cancer **2002**;2(9):683-93.

14. Heiden MGV, Cantley LC, Thompson CB. Understanding the warburg effect: The metabolic requirements of cell proliferation. Science **2009**;324(5930):1029-33 doi 10.1126/science.1160809.

15. Koppenol WH, Bounds PL, Dang CV. Otto Warburg's contributions to current concepts of cancer metabolism. Nat Rev Cancer **2011**;11(5):325-37 doi 10.1038/nrc3038.

16. Kim JW, Dang CV. Cancer's molecular sweet tooth and the warburg effect. Cancer Res **2006**;66(18):8927-30 doi 10.1158/0008-5472.CAN-06-1501.

17. Westerterp M, van Westreenen HL, Reitsma JB, Hoekstra OS, Stoker J, Fockens P, *et al.* Esophageal Cancer: CT, Endoscopic US, and FDG PET for Assessment of Response to Neoadjuvant Therapy—Systematic Review. Radiology **2005**;236(3):841-51 doi 10.1148/radiol.2363041042.

18. Ye Z, Zhu J, Tian M, Zhang H, Zhan H, Zhao C, *et al.* Response of osteogenic sarcoma to neoadjuvant therapy: evaluated by 18F-FDG-PET. Ann Nucl Med **2008**;22(6):475-80 doi 10.1007/s12149-008-0147-y.

19. Bastiaannet E, Groen H, Jager PL, Cobben DCP, van der Graaf WTA, Vaalburg W, *et al.* The value of FDG-PET in the detection, grading and response to therapy of soft tissue and bone

sarcomas; a systematic review and meta-analysis. Cancer Treat Rev **2004**;30(1):83-101 doi 10.1016/j.ctrv.2003.07.004.

20. Jones DN, McCowage GB, Sostman HD, Brizel DM, Layfield L, Charles HC, *et al.* Monitoring of Neoadjuvant Therapy Response of Soft-Tissue and Musculoskeletal Sarcoma Using Fluorine-18-FDG PET. J Nucl Med **1996**;37(9):1438-44.

21. Eschmann SM, Friedel G, Paulsen F, Reimold M, Hehr T, Budach W, *et al.* 18F-FDG PET for assessment of therapy response and preoperative re-evaluation after neoadjuvant radio-chemotherapy in stage III non-small cell lung cancer. Eur J Nucl Med Mol Imaging **2007**;34(4):463-71 doi 10.1007/s00259-006-0273-5.

22. Shields AF, Mankoff DA, Link JM, Graham MM, Eary JF, Kozawa SM, *et al.* Carbon-11-Thymidine and FDG to Measure Therapy Response. J Nucl Med **1998**;39(10):1757-62.

23. de Geus-Oei L-F, Vriens D, van Laarhoven HWM, van der Graaf WTA, Oyen WJG. Monitoring and Predicting Response to Therapy with 18F-FDG PET in Colorectal Cancer: A Systematic Review. J Nucl Med **2009**;50(Suppl 1):43S-54S doi 10.2967/jnumed.108.057224.

24. Schwarz JK, Grigsby PW, Dehdashti F, Delbeke D. The Role of 18F-FDG PET in Assessing Therapy Response in Cancer of the Cervix and Ovaries. J Nucl Med **2009**;50(Suppl 1):64S-73S doi 10.2967/jnumed.108.057257.

25. Andrade RS, Heron DE, Degirmenci B, Filho PAA, Branstetter BF, Seethala RR, *et al.* Posttreatment assessment of response using FDG-PET/CT for patients treated with definitive radiation therapy for head and neck cancers. Int J Radiat Oncol **2006**;65(5):1315-22 doi http://dx.doi.org/10.1016/j.ijrobp.2006.03.015.

26. Yoshioka M, Sato T, Furuya T, Shibata S, Andoh H, Asanuma Y, *et al.* Role of positron emission tomography with 2-deoxy-2-[18F]fluoro-d-glucose in evaluating the effects of arterial infusion chemotherapy and radiotherapy on pancreatic cancer. J Gastroenterol **2004**;39(1):50-5 doi 10.1007/s00535-003-1244-2.

27. Kuwatani M, Kawakami H, Eto K, Haba S, Shiga T, Tamaki N, *et al.* Modalities for Evaluating Chemotherapeutic Efficacy and Survival Time in Patients with Advanced

Pancreatic Cancer: Comparison between FDG-PET, CT, and Serum Tumor Markers. Intern Med **2009**;48(11):867-75 doi 10.2169/internalmedicine.48.2009.

28. Bang S, Chung Hw Fau - Park SW, Park Sw Fau - Chung JB, Chung Jb Fau - Yun M, Yun M Fau - Lee JD, Lee Jd Fau - Song SY, *et al.* The clinical usefulness of 18-fluorodeoxyglucose positron emission tomography in the differential diagnosis, staging, and response evaluation after concurrent chemoradiotherapy for pancreatic cancer. J Clin Gastroenterol **2006**;40(10):923-9.

29. Pery C, Meurette G, Ansquer C, Frampas E, Regenet N. Role and limitations of 18F-FDG positron emission tomography (PET) in the management of patients with pancreatic lesions. Gastroen Clin Biol **2010**;34(8–9):465-74 doi http://dx.doi.org/10.1016/j.gcb.2009.04.014.

30. Higashi T, Saga T, Nakamoto Y, Ishimori T, Fujimoto K, Doi R, *et al.* Diagnosis of pancreatic cancer using fluorine-18 fluorodeoxyglucose positron emission tomography (FDG PET) —Usefulness and limitations in "clinical reality"—. Ann Nucl Med **2003**;17(4):261 doi 10.1007/BF02988521.

31. Strobel O, Buchler MW. Pancreatic cancer: FDG-PET is not useful in early pancreatic cancer diagnosis. Nat Rev Gastroenterol Hepatol **2013**;10(4):203-5.

32. Wilson JM, Mukherjee S, Brunner TB, Partridge M, Hawkins MA. Correlation of 18F-Fluorodeoxyglucose Positron Emission Tomography Parameters with Patterns of Disease Progression in Locally Advanced Pancreatic Cancer after Definitive Chemoradiotherapy. Clin Oncol doi http://dx.doi.org/10.1016/j.clon.2017.01.038.

33. Ghaneh P, Wong W, Titman A, Plumpton C, Vinjamuri S, Johnson C, *et al.* PET-PANC: Multi-centre prospective diagnostic accuracy and clinical value trial of FDG PET/CT in the diagnosis and management of suspected pancreatic cancer. J Clin Oncol **2016**;34:(15 Suppl.).

34. Stefanou DT, Bamias A, Episkopou H, Kyrtopoulos SA, Likka M, Kalampokas T, *et al.* Aberrant DNA Damage Response Pathways May Predict the Outcome of Platinum Chemotherapy in Ovarian Cancer. PLoS ONE **2015**;10(2):e0117654 doi 10.1371/journal.pone.0117654.

35. Goldstein M, Kastan MB. The DNA Damage Response: Implications for Tumor Responses to Radiation and Chemotherapy. Annu Rev Med **2015**;66(1):129-43 doi 10.1146/annurev-med-081313-121208.

36. Hosoya N, Miyagawa K. Targeting DNA damage response in cancer therapy. Cancer Sci **2014**;105(4):370-88 doi 10.1111/cas.12366.

37. Qvarnström OF, Simonsson M, Johansson KA, Nyman J, Turesson I. DNA double strand break quantification in skin biopsies. Radiother Oncol **2004**;72(3):311-7 doi 10.1016/j.radonc.2004.07.009.

38. Dickey JS, Redon CE, Nakamura AJ, Baird BJ, Sedelnikova OA, Bonner WM. H2AX: Functional roles and potential applications. Chromosoma **2009**;118(6):683-92 doi 10.1007/s00412-009-0234-4.

39. Kuo LJ, Yang L-X. γ-H2AX - A Novel Biomarker for DNA Double-strand Breaks. In Vivo **2008**;22(3):305-9.

40. Sharma A, Singh K, Almasan A. Histone H2AX Phosphorylation: A Marker for DNA Damage. In: Bjergbæk L, editor. DNA Repair Protocols. Totowa, NJ: Humana Press; 2012. p 613-26.

41. Nakamura AJ, Rao VA, Pommier Y, Bonner WM. The complexity of phosphorylated H2AX foci formation and DNA repair assembly at DNA double-strand breaks. Cell Cycle **2010**;9(2):389-97 doi 10.4161/cc.9.2.10475.

42. Bonner WM, Redon CE, Dickey JS, Nakamura AJ, Sedelnikova OA, Solier S, *et al.* γH2AX and cancer. Nat Rev Cancer **2008**;8(12):957-67 doi 10.1038/nrc2523.

43. Cornelissen B, Kersemans V, Darbar S, Thompson J, Shah K, Sleeth K, *et al.* Imaging DNA damage in vivo using γH2AX-targeted immunoconjugates. Cancer Res **2011**;71(13):4539-49 doi 10.1158/0008-5472.CAN-10-4587.

44. Cornelissen B, Able S, Kartsonaki C, Kersemans V, Allen PD, Cavallo F, *et al.* Imaging DNA damage allows detection of preneoplasia in the BALB-neuT model of breast cancer. J Nucl Med **2014**;55(12):2026-31 doi 10.2967/jnumed.114.142083.

45. Knight JC, Topping C, Mosley M, Kersemans V, Falzone N, Fernández-Varea JM, *et al.* PET imaging of DNA damage using 89Zr-labelled anti-γH2AX-TAT immunoconjugates. Eur J Nucl Med Mol Imaging **2015**;42(11):1707-17 doi 10.1007/s00259-015-3092-8.

46. Knight JC, Paisey SJ, Dabkowski AM, Marculescu C, Williams AS, Marshall C, *et al.* Scaling-down antibody radiolabeling reactions with zirconium-89. Dalton Trans **2016**;45(15):6343-7 doi 10.1039/C5DT04774A.

47. Reiner T, J. L, Keliher EJ, Yang KS, Ullal A, Kohler RH, *et al.* Imaging Therapeutic PARP Inhibition In Vivo through Bioorthogonally Developed Companion Imaging Agents. Neoplasia **2012**;14:169-77.

48. Maeda H, Nakamura H, Fang J. The EPR effect for macromolecular drug delivery to solid tumors: Improvement of tumor uptake, lowering of systemic toxicity, and distinct tumor imaging in vivo. Adv Drug Deliv Rev **2013**;65(1):71-9 doi 10.1016/j.addr.2012.10.002.

49. Fang J, Nakamura H, Maeda H. The EPR effect: Unique features of tumor blood vessels for drug delivery, factors involved, and limitations and augmentation of the effect. Adv Drug Deliv Rev **2011**;63(3):136-51 doi http://dx.doi.org/10.1016/j.addr.2010.04.009.

50. Freise AC, Wu AM. In vivo imaging with antibodies and engineered fragments. Mol Immunol **2015**;67(2, Part A):142-52 doi http://dx.doi.org/10.1016/j.molimm.2015.04.001.

51. Knight JC, Cornelissen B. Bioorthogonal chemistry: implications for pretargeted nuclear (PET/SPECT) imaging and therapy. Am J Nucl Med Mol Imaging **2014**;4(2):96-113.

52. Cornelissen B, Waller A, Able S, Vallis KA. Molecular radiotherapy using cleavable radioimmunoconjugates that target eGFR and γH2AX. Mol Cancer Ther **2013**;12(11):2472-82 doi 10.1158/1535-7163.

Fig. 1

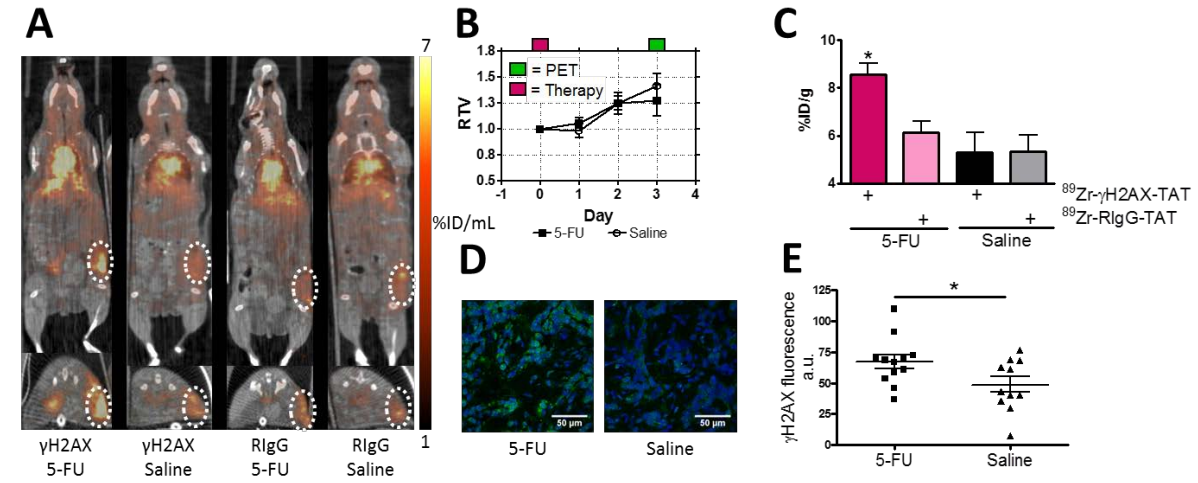
A
7
1
γH2AX 5-FU
γH2AX Saline
RIgG 5-FU
RIgG Saline
B
= PET
= Therapy
RTV
%ID/mL
Day
5-FU
Saline
C
%ID/g
89Zr-γH2AX-TAT
89Zr-RIgG-TAT
5-FU
Saline
D
5-FU
Saline
E
γH2AX fluorescence a.u.
5-FU
Saline

Fig. 2

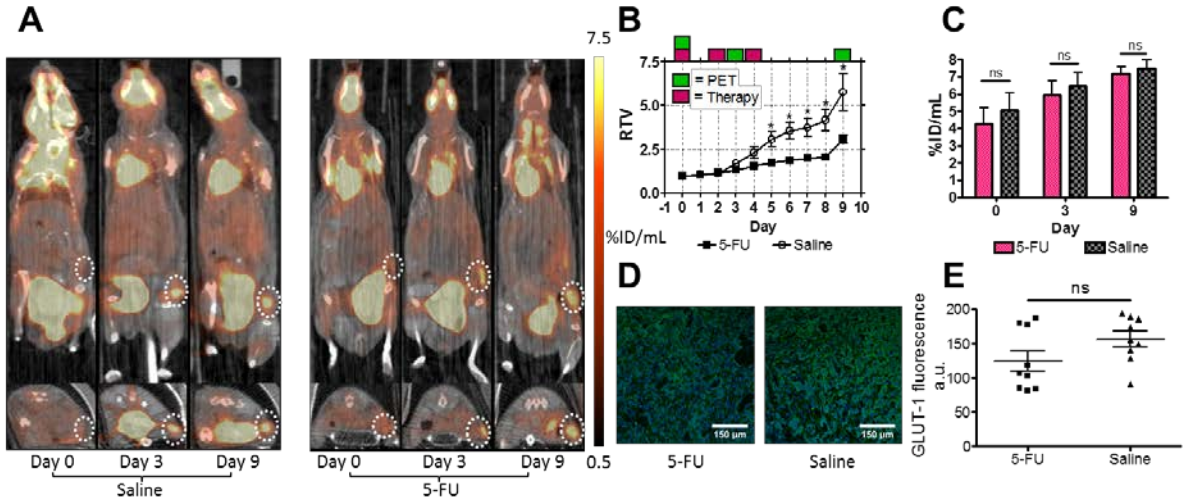
A
7.5
0.5
Day 0
Day 3
Day 9
Saline
5-FU
B
= PET
= Therapy
RTV
%ID/mL
Day
5-FU
Saline
C
ns
%ID/mL
Day
5-FU
Saline
D
5-FU
Saline
E
ns
GLUT-1 fluorescence a.u.
5-FU
Saline

Fig. 3

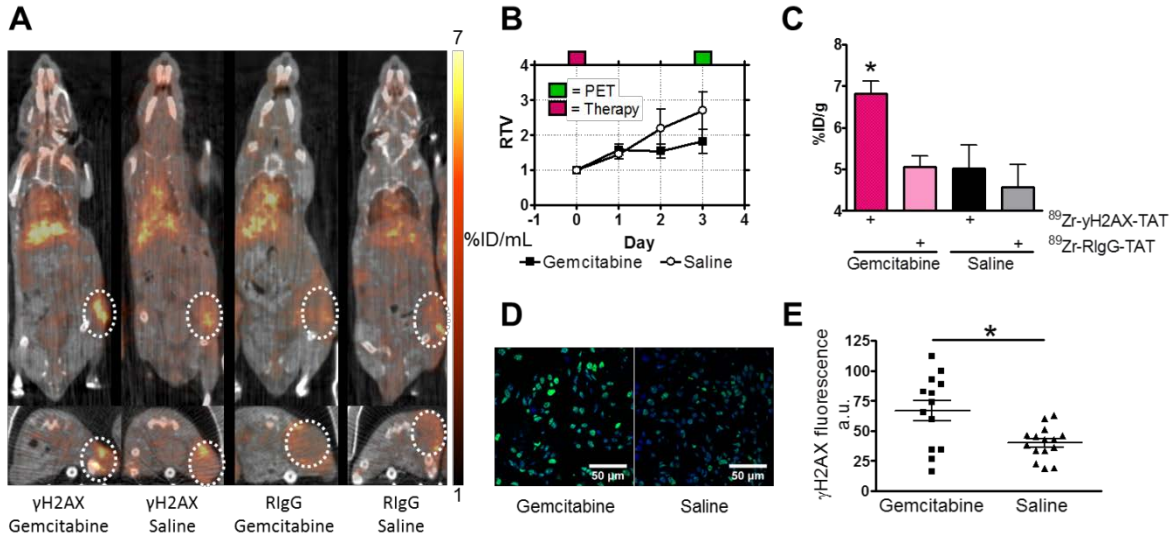
A
7
1
%ID/mL
γH2AX Gemcitabine
γH2AX Saline
RIgG Gemcitabine
RIgG Saline
B
= PET
= Therapy
RTV
Day
Gemcitabine
Saline
C
%ID/g
*
89Zr-γH2AX-TAT
89Zr-RIgG-TAT
Gemcitabine
Saline
D
50 μm
Gemcitabine
Saline
E
γH2AX fluorescence a.u.
*
Gemcitabine
Saline

Fig. 4

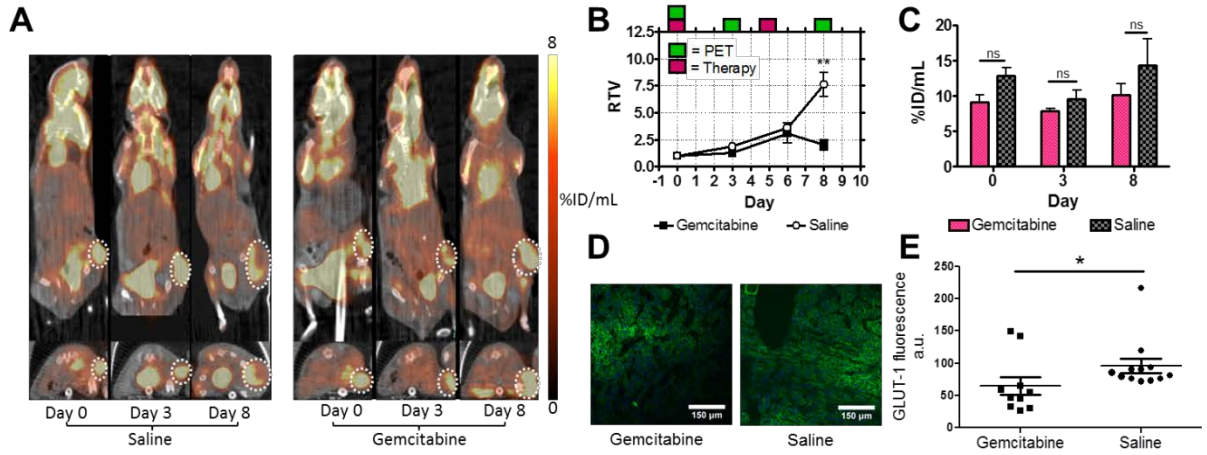
A
8
0
%ID/mL
Day 0
Day 3
Day 8
Saline
Day 0
Day 3
Day 8
Gemcitabine
B
= PET
= Therapy
RTV
**
Day
Gemcitabine
Saline
C
%ID/mL
ns
ns
ns
Day
Gemcitabine
Saline
D
150 μm
150 μm
Gemcitabine
Saline
E
GLUT-1 fluorescence a.u.
*
Gemcitabine
Saline